DOE/ET-53088-393 IFSR #393

Self-Similar Evolution of Nonlinear Magnetic Buoyancy Instability

K. Shibata,[*] *T. Tajima,* and *R. Matsumoto*[†]
Institute for Fusion Studies
The University of Texas at Austin
Austin, Texas 78712

September 1989

[*] *Permanent Address: Department of Earth Sciences, Aichi University of Education, Kariya, Aichi 448, Japan*
[†] *Permanent Address: Department of Information Science, College of Arts and Sciences, Chiba University, Chiba 260, Japan*

Self-Similar Evolution of Nonlinear Magnetic Buoyancy Instability

K. Shibata[a] and T. Tajima
Institute for Fusion Studies
The University of Texas at Austin
Austin, Texas 78712
and
R. Matsumoto
Department of Information Science
College of Arts and Sciences
Chiba University, Chiba 260, Japan

Abstract

A new type of self-similar solutions of ideal magnetohydrodynamics in the nonlinear stage of undular mode ($\mathbf{k}||\mathbf{B}$) of magnetic buoyancy instability (ballooning instability in fusion plasma physic or Parker instability or in astrophysics) are found through MHD simulation and theory. The linear theory developed agrees well with our simulation in the early (linear) stage. The nonlinear stages of the instability in the simulation show the self-similar evolution. One of the solutions obtained from the nonlinear analysis has the characteristics of nonlinear instability in Lagrangian coordinates; the fluid velocity and the Alfvén speed on each magnetic loop increases exponentially with time, because the loop is evacuated by the field aligned motion of matter due to gravitational acceleration. In the later stage of the nonlinear evolution, the solution property

[a]Permanent address: Department of Earth Sciences, Aichi University of Education, Kariya, Aichi 448, Japan

changes from the exponential to the power-law time dependence. The latter corresponds to a force-free expansion solution. The later saturation of velocity increment is also discussed.

PACS numbers: 52.35.Py, 52.65.+z, 96.60.Hv

I. Introduction

A plasma that is supported by a magnetic field under the gravitation is known to be subject to the Kruskal-Schwartzschild (or magnetic Rayleigh-Taylor) instability.[1] Similar instability results in a gravitationally stratified plasma with non-uniform magnetic field, called magnetic buoyancy instability.[2] The magnetic curvature can play a role similar to gravity. The undular mode ($\mathbf{k}\|\mathbf{B}$) of the magnetic buoyancy instability, where $\mathbf{k}$ and $\mathbf{B}$ are the wavenumber and magnetic field vectors, is believed to be important in various physical phenomena ranging from astrophysical plasmas[3] to fusion plasmas,[4] because this mode can be unstable even when the plasma layer is stable against the interchange mode ($\mathbf{k} \perp \mathbf{B}$). For example, for an isothermal case the former is unstable when $dB/dz < 0$, while the latter is unstable only when $d/dz(B/\rho) < 0$, where ρ is the density and the gravitation is in the negative z-direction.

Parker[5] applied the undular instability to the disk of Galaxy. Hence, this instability is called the Parker instability in some astrophysical literatures. The ballooning instability[6] in fusion plasmas has essentially the same physical characteristics as that of the Parker instability with general orientation of $\mathbf{k}$ with respect to $\mathbf{B}$. In spite of many linear theory investigations, however, the physics of nonlinear stages of this instability is much less known.[7] In this paper, we report the discovery of a self-similar solution in the nonlinear stage of the undular instability, which has a characteristics of the *nonlinear instability* (exponential growth in time) in a Lagrangian frame.

In Sec. 2, we summarize basic equations and an initial model. The linear stability of the magnetized plasma in our initial model is studied in Sec. 3, and the results of nonlinear, two-dimensional magnetohydrodynamic (MHD) simulations are discussed in section 4 with emphasis of their self-similar evolutionary pattern. A quasi one-dimensional (1D) self-similar

solution with characteristics of nonlinear instability, which explains simulation results very well, is analytically derived in Sec. 5. In Sec. 6, we consider physical meaning of the results found from simulations and analytical studies, and try to derive basic characteristics of nonlinear evolution of the instability by using an idealized simple model. In Sec. 7 we give a summary and a brief discussion on the comparison of our study with some previous related studies. Finally, in Appendix A we show an exact self-similar solution for the one-dimensional free expansion of a cold magnetized plasma into vacuum, which is useful for understanding of our more complex problems.

II. Basic Equations and Initial Model

We assume that (1) two-dimension (2D) [$V_y = B_y = \partial/\partial y = 0$ in Cartesian coordinate (x, y, z)], (2) ideal magnetohydrodynamics, (3) a constant gravitational acceleration (g) in the negative z-direction. Then, basic equations are:

$$\frac{\partial \rho}{\partial t} + \frac{\partial}{\partial x}(\rho V_x) + \frac{\partial}{\partial z}(\rho V_z) = 0 \ , \tag{1}$$

$$\frac{\partial}{\partial t}(\rho V_x) + \frac{\partial}{\partial x}\left[\rho V_x^2 + p + \frac{1}{8\pi}(B_z^2 - B_x^2)\right] + \frac{\partial}{\partial z}\left(\rho V_x V_z - \frac{1}{4\pi} B_x B_z\right) = 0 \ , \tag{2}$$

$$\frac{\partial}{\partial t}(\rho V_z) + \frac{\partial}{\partial x}\left(\rho V_x V_z - \frac{1}{4\pi} B_x B_z\right) + \frac{\partial}{\partial z}\left[\rho V_z^2 + p + \frac{1}{8\pi}(B_x^2 - B_z^2)\right] + \rho g = 0 \ , \tag{3}$$

$$\frac{\partial B_x}{\partial t} + \frac{\partial}{\partial z}\left(V_z B_x - V_x B_z\right) = 0 \ , \tag{4}$$

$$\frac{\partial B_z}{\partial t} - \frac{\partial}{\partial x}\left(V_z B_x - V_x B_z\right) = 0 \ , \tag{5}$$

$$\begin{aligned} &\frac{\partial}{\partial t}\left[\frac{p}{\gamma - 1} + \frac{1}{2}\rho(V_x^2 + V_z^2) + \frac{1}{8\pi}(B_x^2 + B_z^2)\right] \\ &+\frac{\partial}{\partial x}\left[\frac{\gamma}{\gamma - 1} p V_x + \frac{1}{2}\rho V_x (V_x^2 + V_z^2) + \frac{B_z}{4\pi}(V_x B_z - V_z B_x)\right] \\ &+\frac{\partial}{\partial z}\left[\frac{\gamma}{\gamma - 1} p V_z + \frac{1}{2}\rho V_z (V_x^2 + V_z^2) + \frac{B_x}{4\pi}(V_z B_x - V_x B_z)\right] \\ &+\rho g V_z = 0 \ , \end{aligned} \tag{6}$$

where γ is a specific heat ratio and is assumed to be 1.05 in this paper because the growth rate of the undular mode of the magnetic buoyancy instability is larger for smaller γ.[3,5]

The initial gas layer is in magneto-static equilibrium and consists of a cold isothermal plasma layer, which is partly permeated by horizontal isolated magnetic flux sheet in $z_0 < z < z_0 + D$, and a hot isothermal, non-magnetized plasma layer above the cold layer. Hereafter, the units of length, velocity, and time are H, C_s, and H/C_s, where $H = C_s^2/(\gamma g)$ is the scale height and C_s is the sound speed in the cold layer. The temperature distribution is taken to be

$$T(z) = T_1 + (T_2 - T_1)\left[\tanh\left((z - z_{tr})/w_{tr}\right) + 1\right]/2 \ , \tag{7}$$

where T_2/T_1 (which is assumed to be=25 here) is the ratio of the temperature in the hot layer to that in the cold layer, z_{tr} is the height of the transition layer between the cold and hot layers, w_{tr} is the temperature scale height in the transition layer ($= 0.6H$ for all our calculations, where H is the pressure scale height of the cold layer).

We assume that the magnetic field is initially parallel to the horizontal plane; $\mathbf{B} = (B_x(z), 0, 0)$, and is localized in the cold layer. The distribution of magnetic field strength is given by

$$B_x(z) = [8\pi p(z)/\beta(z)]^{1/2} \ ,$$

where

$$\beta(z) = \beta_*/f(z) \ , \tag{8}$$

$$f(z) = \left[\tanh\left((z - z_0)/w_0\right) + 1\right]\left[-\tanh\left((z - z_1)/w_1\right) + 1\right]/4 \ .$$

Here, β_* is the ratio of gas pressure to magnetic pressure at the center of the magnetic flux sheet, z_0 and $z_1 = z_0 + D$ are the heights of the lower and upper boundary of the magnetic flux sheet, D is the vertical thickness of the magnetic flux sheet. It is assumed that $z_0 = 0$, $D = 4H$, $w_0 = w_1 = 0.5H$, $w_2 = 0.6H, \beta_* = 1$ for all of our calculations.

On the basis of the above initial plasma β distribution, the initial density and pressure distributions are numerically calculated by the equation of static pressure balance

$$\frac{d}{dz}\left[p+\frac{B_x^2(z)}{8\pi}\right]+\rho g=0\ . \tag{9}$$

We assume periodic boundary for $x=0$ and $X_{\max}(=80)$, conducting wall boundary for $z=0$, and free boundary for $z=Z_{\max}(=35)$.

III. Linear Stability Analysis

We here study the main characteristics of the linear instability of an isolated magnetic flux sheet described in Sec. 2. We perform a linear stability analysis using the normal mode method similar to those of Horiuchi *et al.*[8] That is, we first linearize the basic equations (1)–(6) by assuming $B_x=B_0+b_x$, $|b_x/B_0|\ll 1$, and $b_x=\tilde{b}_x\exp(i\omega t+ik_x x+ik_y y)$, etc. After some manipulations, the linearized equations become

$$\frac{d}{dz}\begin{bmatrix}\xi\\ \eta\end{bmatrix}=\begin{bmatrix}D_{\xi\xi} & D_{\xi\eta}\\ D_{\eta\xi} & D_{\eta\eta}\end{bmatrix}\begin{bmatrix}\xi\\ \eta\end{bmatrix}, \tag{1}$$

where

$$D_{\xi\xi}=\frac{1}{1+\beta}\frac{d\ln\beta}{dz}\frac{d\ln T}{dz}$$
$$-\frac{g}{C_s^2}\frac{\beta\gamma}{1+\beta}\frac{(1+\beta\gamma-\beta)\omega^2-2k_x^2C_s^2}{(2+\beta\gamma)\omega^2-2k_x^2C_s^2}\ , \tag{2}$$

$$D_{\xi\eta}=-\frac{\beta\gamma}{C_s^2}\frac{\beta\gamma\omega^4-\omega^2(2+\beta\gamma)k^2C_s^2+2k^2k_x^2C_s^4}{[(2+\beta\gamma)\omega^2-2k_x^2C_s^2][\beta\gamma\omega^2-2k_x^2C_s^2]}\ , \tag{3}$$

$$D_{\eta\xi}=\omega^2-\frac{2}{\beta\gamma}k_x^2C_s^2+g\left(\frac{1}{1+\beta}\frac{d\ln\beta}{dz}-\frac{d\ln T}{dz}\right)$$
$$-\frac{1}{1+\beta}\frac{g^2}{C_s^2}\frac{\beta\gamma(1+\beta\gamma-\beta)\omega^2+2(1+\beta-\beta\gamma)k_x^2C_s^2}{(2+\beta\gamma)\omega^2-2k_x^2C_s^2}\ , \tag{4}$$

$$D_{\eta\eta}=-\frac{g}{C_s^2}\frac{\beta\gamma\omega^2}{(2+\beta\gamma)\omega^2-2k_x^2C_s^2}\ , \tag{5}$$

and

$$\xi = \rho_0 \tilde{v}_z,$$

$$\eta = i\omega \left(\delta\tilde{p} + \frac{B_0 \tilde{b}_x}{4\pi} \right) ,$$

$$k^2 = k_x^2 + k_y^2 ,$$

and ρ_0 and B_0 are the quantities in the unperturbed state, and $\tilde{v}_z$, $\delta\tilde{p}$, $\tilde{b}_x$ are perturbed quantities. Here, we used the equation (10) of magnetostatic balance for the unperturbed quantities, and $T = T(z)$ and $\beta = \beta(z)$ are given in equations (7) and (8).

The boundary conditions are $\xi = 0$ and $d\eta/dz = 0$ on $z = 0$, and ξ and η should vanish at $z \to \infty$. The equations (10)–(14) are solved numerically for prescribed k_x and k_y using the Runge-Kutta method to find an eigenvalue ω and the corresponding eigenfunctions which satisfy these boundary conditions.

Figure 1 shows the growth rates $i\omega$ as a function of the horizontal wavenumber k_x for three cases $\beta_* = 0.5$, 1.0, and 2.0 for $k_y = 0$. It is seen that the instability occurs if the horizontal wavelength, λ, is larger than the critical wavelength, $\lambda_c \simeq 14H$ for $\beta_* = 1$. (If $D = \infty$ and $\gamma = 1$, the critical wavelength is analytically calculated; $\lambda_c \simeq 4\pi H/(1+2/\beta_*)^{1/2}$).[3,5] The most unstable wavelength is $\simeq 20H$ ($k_x = 0.314$) for $\beta_* = 1$. The growth rates for $\beta_* = 0.001$, 0.5, 1, and 2 when $k_x = 0.314$ and $k_y = 0$ are 0.19, 0.15, 0.12, and 0.08, respectively. From these numerical results, we can construct an empirical, approximate formula for the growth rates (for $\beta_* \leq 2$);

$$\omega_l \simeq 0.2(1 + 2\beta_*)^{-1/2} C_s/H , \tag{15}$$

It is seen that the growth rates tend to a non-zero value when β_* becomes 0 for finite D. This behavior is quite different from that for the case of a non-isolated field,[5,7] where the growth rates tend to zero when β_* becomes 0. This is because in the case of isolated field the density is locally larger just above the flux sheet than in the sheet, i.e., the density inversion

occurs locally as in the case of a familiar magnetic Rayleigh-Taylor instability.[1–3]

Figure 2 shows the 1D eigenfunctions (as a function of z) for some physical quantities. It is noted that both velocities $\tilde{v}_x$ and $\tilde{v}_z$ are maximum at the height near the top of the flux sheet ($z \simeq 8$), and that they have non-negligible values even above the flux sheet. The same is true for the magnetic field, density and gas pressure.

IV. Nonlinear Simulations

The MHD equations with $\gamma = 1.05$ are solved numerically by using modified Lax-Wendroff scheme with artificial viscosity.[9,10] We initially give the system small-amplitude perturbations ($V_{\max} = 0.01 C_s$) having the same spatial distributions as those of linear eigenfunctions in the unstable mode with $\lambda = 20H$ in the finite horizontal domain ($X_{\max}/2 - \lambda/2 < x < X_{\max}/2 + \lambda/2$).

Figure 3 shows the time evolution of magnetic lines of force, the velocity field, and the density distribution. As the magnetic loop rises, the gas slides down along the loop. Spikes of dense regions are created on the valleys of the undulating field lines, whereas the rarefied regions are produced around the top of magnetic loops. The most salient characteristics in the nonlinear stage ($t > 40$) is the approximate *self-similar pattern* of magnetic loop expansion; the rise velocity of the magnetic loop and the velocity of downflow along the loop increase with height as the loop expands and ascends. Figure 4 shows some physical quantities at $x = X_{\max}/2$ (midpoint of the magnetic loops), indicating approximate self-similar behavior as a function of height. We also find

$$V_z = az \quad ; \quad V_A = a_2 z \ , \tag{16}$$

where $a \simeq 0.06$ (for $t < 60$), $a_2 \simeq 0.3$, and z is the height measured from $z_0 (= 4)$.[1] On the

[1]Note that hereafter we often use z as the height from $z_0 = 4$, the base of the magnetic flux sheet, instead of the height from the bottom of the computing box when discussing the self-similar behavior of the magnetic flux expansion. However, the latter definition is used in all figures of simulation results.

other hand, we find the density and magnetic field strength have the power-law distribution;

$$\rho \propto z^{-4} \quad ; \quad B_x \propto z^{-1} \, . \tag{17}$$

Figure 5 shows the time evolution of the Lagrangian displacement of a test particle at the midpoint of the loop in the simulation results. In the initial stage, the growth rate of the perturbation amplitude agrees well with linear theoretical values ($\omega_l = 0.12$). The amplitude increases exponentially with time even in the nonlinear stage ($t > 40$); $z \propto \exp(\omega_n t)$ and $\omega_n \simeq a \simeq 0.06 \simeq \omega_l/2$.

V. Self-Similar Solution

A. Nonlinear Instability

We shall now look for a self-similar solution of the problem by analytical method. We have the following relation from Eq. (16); $\partial V_z/\partial \tau = \partial V_z/\partial t + V_z \partial V_z/\partial z = a V_z$, where τ is the time in Lagrangian coordinates, while t and z are the Eulerian coordinates. This leads to

$$V_z(\xi, \tau) = a\xi \exp(a\tau) \, , \tag{18}$$

where $\xi = z \exp(-a\tau)$ is the Lagrangian coordinate.

We assume the quasi one-dimension (1D) for the problem, i.e., we consider only vertical (z)-variation of the physical quantities at the midpoint of the loop. The basic equations of our quasi-1D problem are

$$\frac{\partial \rho}{\partial t} = -\frac{\partial}{\partial z}(\rho V_z) - \frac{\partial}{\partial z}(\rho V_x) \, , \tag{19}$$

$$\rho \left(\frac{\partial V_z}{\partial t} + V_z \frac{\partial V_z}{\partial z} \right) = -\left[\frac{\partial}{\partial z} \left(\frac{B_x^2}{8\pi} \right) + \frac{B_x^2}{4\pi R} \right] \, , \tag{20}$$

$$\frac{\partial B_x}{\partial t} = -\frac{\partial}{\partial z}(B_x V_z) \, , \tag{21}$$

where R is the radius of curvature of field lines at the midpoint of the magnetic loop. The last term on the right hand side of Eq. (20) is in a simplified phenomenological form in order to

keep the variation in one (z)-direction. Here we neglect the gas pressure and the gravitational forces in Eq. (20), and the reason will become clear after the self-similar solutions are found. The neglect of B_z-related term in Eq. (21) may be justified because $B_z \ll B_x$ near the midpoint of the magnetic loop. A central Anzatz of the present quasi-1D model is

$$\partial(\rho V_x)/\partial x = (N-1)\partial(\rho V_z)/\partial z \ , \tag{22}$$

where N is assumed to be constant. The left-hand term in Eq. (22) corresponds to fluid leaking along the field line away from the midsection of the loop because the bent loop allows the fluid to escape under the gravitational influence. Here, we measure the amount of matter leakage in the horizontal direction in terms of the vertical flow motion. If $N = 1$, no leakage arises, which corresponds to a pure 1D motion. In order to have matter leakage, $N < 1$. $N - 1$ is a parameter that measures severity of matter leakage in the x-direction.

We further assume $R = cz$ and $c = constant$, which is a manifestation of the self-similar evolution of the spatial pattern of the loop, as observed in Fig. 3(c).

Under these assumptions, a particular self-similar solution, that satisfies our empirical velocity functions (16) and (18) and quasi-1D MHD equations (19)–(21), is found;

$$\rho = \sigma_1 \xi^{-4-2q} \exp(-4a\tau) = \sigma_1 z^{-4-2q} \exp(2qat) \ , \tag{23}$$

$$B_x = b_1 \xi^{-1-q} \exp(-a\tau) = b_1 z^{-1-q} \exp(qat) \ , \tag{24}$$

where $q = 3N/[2(1-N)]$, $\sigma_1 = \sigma(\xi = 1)$, $b_1 = a[4\pi r_1/(q+1-1/c)]^{1/2}$. The simulation results (17) [see Figs. 4(c) and (d)] indicate the analytical solution with $N = q = 0$, which leads to a steady solution in Eulerian coordinates in Eqs. (23)–(24). The physical reason why we obtain $N \simeq 0$ will be explained in Sec. 6. Our self-similar solution leads to $\rho g/[\partial/\partial z(B_x^2/8\pi)] \propto z^{-1}$ and $\partial p/\partial z/[\partial/\partial z(B_x^2/8\pi)] \simeq (C_s/V_A)^2 \propto z^{-2}$. Hence, as the magnetic loop rises, both forces decrease more rapidly than the magnetic force; as long as above force ratios are less than unity at $t = 0$, the neglect of the gravitational and the gas pressure forces in the nonlinear

evolution is valid, while the nonlinear growth rate a is found to be related g (see Eq. (101) in Sec. 6.3).

B. General Self-Similar Analysis and Solutions

In this subsection, we shall show that there is another class of self-similar solutions with power-law time dependence, in addition to the empirical solution with exponential time dependence discussed in the previous subsection.

We further consider why V_z is proportional to z. Table 1 summarizes solutions found in this subsection. One of the power-law solutions has the characteristics that $V_z \propto z/t$, $\rho \propto z^{-4}$, $B_x \propto z^{-1}$, and explains the behavior of simulation results after $t > 60$ in Fig. 4(a); after the magnetic loop enters the hot layer.

In contrast to the previous subsection and Shibata *et al.*,[10] we here use the cylindrical coordinate (r, θ, y), where r is the radial distance from the point $(X_{\max}/2, z_0)$, z_0 is the base height of the initial magnetic flux sheet, and θ is the angle measured from the vertical line towards the positive x-direction. (Hence we have $r \simeq z$ for $|\theta| \ll 1$) This is because the magnetic field configuration tends to have the current free configuration of $(B_r, B_\theta, B_y) \propto (1/r, 0, 0)$ as time proceeds, so that the equation becomes simpler in the cylindrical coordinate than in the Cartesian coordinate. We also find a new solution, a force-free solution, which are not found in the previous analysis.[10]

We now write the quasi-1D equations (19)-(21) in the cylindrical coordinate.

$$\frac{\partial \rho}{\partial t} = -\frac{\partial}{r\partial r}(r\rho V_r) - \frac{\partial}{r\partial \theta}(\rho V_\theta) \ , \tag{25}$$

$$\rho\left(\frac{\partial V_r}{\partial t} + V_r\frac{\partial V_r}{\partial r}\right) = -\left[\frac{\partial}{\partial r}\left(\frac{B_t h^2}{8\pi}\right) + \frac{B_\theta^2}{4\pi R}\right] \ , \tag{26}$$

$$\frac{\partial B_\theta}{\partial t} = -\frac{\partial}{\partial r}(B_\theta V_r) \ , \tag{27}$$

and we assume again $R = cr$, and

$$\frac{\partial}{r\partial \theta}(\rho V_\theta) = (N-1)\frac{\partial}{r\partial r}(r\rho V_r) \ .$$

As in the standard self-similar analysis,[11,12,13] we seek a general self-similar solution by adopting the new dimensionless independent variable

$$\zeta = \frac{r}{Z(t)} , \tag{28}$$

$$\tau = \frac{t}{t_0} , \tag{29}$$

where $Z(t)$ is the scale function, with dimension of length, and t_0 is a normalization constant for the time. We further assume

$$V_r = \dot{Z}(\tau) v(\zeta)/t_0 , \tag{30}$$

$$\rho = \Sigma(\tau)\sigma(\zeta), \tag{31}$$

$$B_\theta = (4\pi\Sigma\dot{Z}^2)^{1/2} b(\zeta)/t_0 , \tag{32}$$

where v, σ, and b are nondimensional quantities with only ζ-dependence, and the dot represents $d/d\tau$. Substituting Eqs. (28)–(32) into Eqs. (25)–(27), we have

$$\frac{\dot{\Sigma}}{\Sigma}\frac{Z}{\dot{Z}} + Nv' + N\frac{v}{\zeta} + (Nv - \zeta)\frac{\sigma'}{\sigma} = 0 , \tag{33}$$

$$\frac{Z\ddot{Z}}{\dot{Z}^2} v + (v - \zeta)v' + \frac{b^2}{\sigma}\left(\frac{b'}{b} + \frac{1}{c\zeta}\right) = 0, \tag{34}$$

$$\frac{Z\ddot{Z}}{\dot{Z}^2} + \frac{1}{2}\frac{\dot{\Sigma}}{\Sigma}\frac{Z}{\dot{Z}} + (v - \zeta)\frac{b'}{b} + v' = 0 , \tag{35}$$

where $' \equiv d/d\zeta$.

We adopt the boundary condition for $v(\zeta)$

$$v(\zeta = 0) = 0 \tag{36}$$

because there is no magnetic flux below $\zeta = 0$, and thus the fluid is stationary there. Thus, $v(\zeta)$ may be written as a self-similar function that satisfies Eq. (36),

$$v(\zeta) = \zeta^\delta , \tag{37}$$

where δ is a positive real number. We now consider the solution of Eqs. (33)–(35) for boundary condition (36) for both $Z\ddot{Z}/\dot{Z}^2 = 1$ and $\neq 1$.

a) Case $Z\ddot{Z}/\dot{Z}^2 \neq 1$

In this case, Z may be written as

$$Z = Z_0 \tau^\alpha \,, \tag{38}$$

where Z_0 is a normalization constant. We also assume that Σ has a similar power-law dependence on τ,

$$\Sigma = \Sigma_0 \tau^\beta \,, \tag{39}$$

where Σ_0 is a density normalization constant. We consider two separate cases, $\delta \neq 1$ and $\delta = 1$.

i) $\delta \neq 1$

Equation (35) can be written, by using Eqs. (37), (38), (39), as

$$\frac{b'}{b} = \frac{\frac{\alpha-1}{\alpha} + \frac{\beta}{2\alpha} + v'}{\zeta - v} = \frac{\frac{\alpha-1}{\alpha} + \frac{\beta}{2\alpha} + \delta\zeta^{\delta-1}}{\zeta(1-\zeta^{\delta-1})} \,. \tag{40}$$

The right hand side of equation (40) diverges at $\zeta = 1$ unless the numerator vanishes when the denominator vanishes. Thus, we impose

$$\frac{\alpha-1}{\alpha} + \frac{\beta}{2\alpha} = -\delta \,, \tag{41}$$

which yields

$$\frac{b'}{b} = -\frac{\delta}{\zeta} \,. \tag{42}$$

It follows from equation (42) that

$$b = b_1 \zeta^{-\delta} \,, \tag{43}$$

with b_1 a constant. Similarly, Eq. (33) reads

$$\frac{\sigma'}{\sigma} = \frac{\frac{\beta}{\alpha} + N(v' + \frac{v}{\zeta})}{\zeta - Nv} \,. \tag{44}$$

If $N \neq 0$, the solution of Eq. (44) becomes

$$\sigma = \sigma_1 \zeta^{-\delta}, \tag{45}$$

and $\beta/\alpha = -(1+\delta)$, where σ_1 is a constant. Inserting Eqs. (43) and (45) into Eq. (34), we obtain

$$\frac{\alpha - 1}{\alpha} + \delta(\zeta^{\delta - 1} - 1) + \frac{b_1^2}{\sigma_1} \zeta^{-2\delta - 1} \left(\frac{1}{c} - \delta \right) = 0 \,. \tag{46}$$

It is apparent that the left-hand side is not identically equal to zero. Thus, when $N \neq 0$, there is no solution with $\delta \neq 1$. Physically speaking, the solution with $\delta \neq 1$ diverges at a finite distance from the origin, so that such a solution is not acceptable.

On the other hand, Eq. (34) with $N = 0$ yields the solution

$$\sigma = \sigma_1 \zeta^{\frac{\beta}{\alpha}} \,. \tag{47}$$

Note that Eq. (47) differs from Eq. (45) because β/α is not necessarily equal to $-(1+\delta)$ for Eq. (47). Inserting Eqs. (43) and (47) into Eq. (34), we have

$$\frac{\alpha - 1}{\alpha} + \delta(\zeta^{\delta - 1} - 1) + \frac{b_1^2}{\sigma_1} \zeta^{-3\delta - \frac{\beta}{\alpha} - 1} \left(\frac{1}{c} - \delta \right) = 0 \,. \tag{48}$$

This equation is identically satisfied when

$$\frac{\alpha - 1}{\alpha} - \delta = 0 \,, \tag{49}$$

$$-3\delta - \frac{\beta}{\alpha} - 1 = \delta - 1 \,, \tag{50}$$

$$\delta + \frac{b_1^2}{\sigma_1} \left(\frac{1}{c} - \delta \right) = 0 \,. \tag{51}$$

From Eqs. (49) and (50), we have $\alpha = 1/(1-\delta)$, and $\beta/\alpha = -4\delta$. The solution for $N = 0$ is summarized as follows:

$$V_r = \alpha \frac{Z_0}{t_0} \tau^{\alpha-1} \zeta^{\frac{\alpha-1}{\alpha}} = \alpha \frac{Z_0}{t_0} \left(\frac{r}{Z_0}\right)^{\frac{\alpha-1}{\alpha}} , \tag{52}$$

$$\rho = \Sigma_0 \sigma_1 \tau^{-4(\alpha-1)} \zeta^{-4\left(\frac{\alpha-1}{\alpha}\right)} = \Sigma_0 \sigma_1 \left(\frac{r}{Z_0}\right)^{-4\left(\frac{\alpha-1}{\alpha}\right)} , \tag{53}$$

$$B_\theta = B_0 b_1 \tau^{-(\alpha-1)} \zeta^{-\left(\frac{\alpha-1}{\alpha}\right)} = B_0 b_1 \left(\frac{r}{Z_0}\right)^{-\left(\frac{\alpha-1}{\alpha}\right)} , \tag{54}$$

where $B_0 = (\alpha Z_0/t_0)(4\pi\Sigma_0)^{1/2}$, $b_1 = [\delta\sigma_1/(\delta - 1/c)]^{1/2}$, and $\delta = (\alpha-1)/\alpha$.

Note that (τ, ζ) are Lagrangian coordinates, and Eqs. (52)–(54) are steady solutions in Eulerian coordinates. We consider only an expansion flow $Z = Z_0 \tau^\alpha$ with $\alpha > 0$. In this case the solution with $\delta > 1$ is not permitted. However, if we assume

$$Z = Z_0(\tau_c - \tau)^\alpha Z_0 \frac{1}{(\tau_c - \tau)^{\frac{1}{\delta-1}}} , \tag{55}$$

$$\Sigma = \Sigma_0 (\tau_c - \tau)^\beta , \tag{56}$$

for $\alpha < 0$ or $\delta > 1$ instead of Eqs. (38) and (39), the solutions (52)–(54) are applied for $\delta > 1$. Here, τ_c is a non-zero constant depending on the initial condition. In this case, τ in Eqs. (52)–(54) should be replaced with $(\tau_c - \tau)$, and the Lagrangian velocity is

$$V_r \propto (\tau_c - \tau)^{\alpha-1} = \frac{1}{(\tau_c - \tau)^{\frac{\delta}{\delta-1}}} , \tag{57}$$

so that the velocity becomes infinite in a finite time.

On the other hand, when $\delta \to 1 (\alpha \to \infty)$, the solution becomes $V_r \propto r$, $\rho \propto r^{-4}$, $B_\theta \propto r^{-1}$. The dependence on r of these solutions is the same as in our empirical self-similar solutions with exponential time dependence (see Sec. 6.1 and b.ii).

ii) $\delta = 1$

In this case the basic equations become

$$\frac{\beta}{\alpha} + 2N + (N-1)\zeta\frac{\sigma'}{\sigma} = 0 \ , \tag{58}$$

$$\frac{\alpha-1}{\alpha}\zeta + \frac{b^2}{\sigma}\left(\frac{b'}{b} + \frac{1}{c\zeta}\right) = 0 \ , \tag{59}$$

$$\frac{\alpha-1}{\alpha} + \frac{\beta}{2\alpha} + 1 = 0 \ . \tag{60}$$

Thus, when $N \neq 1$, we obtain

$$\beta = 2 - 4\alpha \ , \tag{61}$$

$$\sigma = \sigma_1 \zeta^{-4-2h} \ , \tag{62}$$

$$b = b_1 \zeta^{-1-h} \ , \tag{63}$$

where the constants are defined as $h = (N - 1/\alpha)/(1-N)$, and $b_1 = [\sigma_1(1-\alpha)/\alpha/(-1 - h + 1/c)]^{1/2}$. Then Eqs. (30)–(32) give rise to

$$V_r = \alpha\frac{Z_0}{t_0}\tau^{\alpha-1}\zeta = \alpha\frac{r}{t} \ , \tag{64}$$

$$\rho = \Sigma_0\sigma_1\tau^{2-4\alpha}\zeta^{-4-2h} = \Sigma_0\sigma_1\left(\frac{t}{t_0}\right)^{2(1+h\alpha)}\left(\frac{r}{Z_0}\right)^{-4-2h} \ , \tag{65}$$

$$B_\theta = B_0 b_1 \tau^{-}\alpha\zeta^{-1-h} = B_0 b_1\left(\frac{t}{t_0}\right)^{h\alpha}\left(\frac{r}{Z_0}\right)^{-1-h} \ . \tag{66}$$

It should be noted that the coordinates (τ, ζ) are Lagrangian coordinates.

When $N = 1$, we have the following solution for $c = 1$,

$$\alpha = 1 \ , \tag{67}$$

$$\beta = -2 \ , \tag{68}$$

$$V_r = \frac{Z_0}{t_0}\zeta = \frac{r}{t} \ , \tag{69}$$

$$\rho = \Sigma_0\sigma_1\tau^{-2}\zeta^{-\mu} = \Sigma_0\sigma_1\left(\frac{t}{t_0}\right)^{\mu-2}\left(\frac{r}{Z_0}\right)^{-\mu} \ , \tag{70}$$

$$B_\theta = B_0 b_1 \tau^{-1} \zeta^{-1} = B_0 b_1 \left(\frac{r}{Z_0}\right)^{-1} \tag{71}$$

where $B_0 = (4\pi\Sigma_0)^{1/2} Z_0/t_0$, $V_A = r/t$, and μ is an arbitrary constant. This freedom comes from the decoupling of the inertial term and the magnetic force term in the equation of motion, Eq. (59), because the inertial term becomes exactly equal to 0. This solution belongs to a force-free ($\mathbf{J} \times \mathbf{B} = 0$) solution, and we will study more general force-free solutions in Sec. 6.2.c.

b) Case $Z\ddot{Z}/\dot{Z}^2 = 1$

In this case, we have the solution varying as

$$Z = Z_0 \exp(a\tau) \ . \tag{72}$$

We assume that the density Σ also has exponential time dependence,

$$\Sigma = \Sigma_0 \exp(n\tau) \ . \tag{73}$$

i) $\delta \neq 1$

The formulation and results are similar to those for $N \neq 1$ of a.i; there is no solution with $\delta \neq 1$. It should be noted that there are no solutions with $\delta \neq 1$ even for $N = 0$ in this case.

ii) $\delta = 1$

The basic equations are

$$\frac{n}{a} + 2N + (N-1)\zeta \frac{\sigma'}{\sigma} = 0 \ , \tag{74}$$

$$\zeta + \frac{b^2}{\sigma}\left(\frac{b'}{b} + \frac{1}{c\zeta}\right) = 0 \ , \tag{75}$$

$$2 + \frac{1}{2}\frac{n}{a} = 0 \ . \tag{76}$$

Thus for $N \neq 1$ we have

$$\frac{n}{a} = -4 \ , \tag{77}$$

$$\sigma = \sigma_1 \zeta^{-4-2p} \ , \tag{78}$$

and

$$b = b_1 \zeta^{-1-p} \ , \tag{79}$$

where $p = N/(1-N)$, and $b_1 = [\sigma_1/[1/(1-N) - (1/c)]]^{1/2}$. The solution is summarized as follows:

$$V_r = (aZ_0/t_0)\zeta \exp(a\tau) = (a/t_0)r \ . \tag{80}$$

$$\rho = \Sigma_0 \sigma_1 \zeta^{-4-2p} \exp(-4a\tau) = \Sigma_0 \sigma_1 \left(\frac{r}{Z_0}\right)^{-4-2p} \exp\left[2pa\frac{t}{t_0}\right] \ , \tag{81}$$

$$B_\theta = B_0 b_1 \zeta^{-1-p} \exp(-a\tau) = B_0 b_1 \left(\frac{r}{Z_0}\right)^{-1-p} \exp\left[pa\frac{t}{t_0}\right] \ . \tag{82}$$

This exponential solution, which is one of the four possible solutions (Table 1), is essentially the same as our empirical solution in Sec. 6.1 (23) and (24). (Note that $p = N/(1-N)$ is different from $q = 3N/2(1-N)$ in Eqs. (23) and (24) because the geometry is different.) It should be noted that there is no solution for $N = 1$ in this exponential case.

c) Force-free solutions

Let us now consider force-free solutions, i.e., solutions satisfying $\mathbf{J} \times \mathbf{B} = 0$. In this case, the inertial term dV_r/dt becomes identically zero, since we assumed that the gravity and the pressure force are neglected. Thus we have

$$V_r = r/t \ . \tag{83}$$

Equivalently, the following functions

$$Z = Z_0 \tau \ , \tag{84}$$

$$v = \zeta \ , \tag{85}$$

satisfy the force-free condition as evident from equation (34). (Note that Eq. (84) corresponds to $\alpha = 1$ in (38).) From the condition that the third term should vanish in Eq. (34), we obtain

$$c = 1 \quad , \quad b = b_1/\zeta \ , \tag{86}$$

where b_1 is an arbitrary constant.

Since the inertial term and the $\mathbf{J} \times \mathbf{B}$ term decouple in the equation of motion, we do not have to assume equation (32), so that we may write

$$B_\theta = W(\tau) b(\zeta) \ . \tag{87}$$

Hence Eq. (35) is replaced by

$$\frac{\dot{W}}{W}\frac{Z}{\dot{Z}} + (v - \zeta)\frac{b'}{b} + v' = 0 \ . \tag{88}$$

Inserting Eqs. (85)–(87) into (88), and assuming

$$W = W_0 \tau^\nu \ , \tag{89}$$

we find

$$\nu = -1 \ . \tag{90}$$

On the other hand, Eq. (33) becomes

$$\beta + 2N + (N-1)\zeta\frac{\sigma'}{\sigma} = 0 \ . \tag{89}$$

When $N = 1$, this equation leads to $\beta = -2$. Therefore the solutions in this case are essentially the same as Eqs. (67)–(71). When $N \neq 1$, from (89) we have

$$\sigma = \sigma_1 \zeta^{\beta + w} \ , \tag{90}$$

where $w = (\beta + 2)N/(1 - N)$. The solutions are summarized as follows:

$$V_r = (Z_0/t_0)\zeta = r/t \ , \tag{91}$$

$$B_\theta = W_0 b_1 \tau^{-1} \zeta^{-1} = W_0 b_1 (r/Z_0)^{-1} , \tag{92}$$

$$\rho = \Sigma_0 \sigma_1 \tau^\beta \zeta^{\beta+w} = \Sigma_0 \sigma_1 t^{-w} r^{\beta+w} . \tag{93}$$

The force-free solution for $N = 1$ described above corresponds to a one-dimensional version of Low's[14] two-dimensional self-similar solution, although he did not discuss the solution with $N \neq 1$, i.e., the solution with downflows.

VI. Physical Interpretation of Numerical and Analytical Results

A. Classification of Evolutional Stage by Curvature Radius of Magnetic Field Lines

On the basis of numerical and analytical results obtained in previous sections, we can construct a rough model of linear-nonlinear evolution of the undular mode of the magnetic buoyancy instability. A key physical parameter is R, a curvature radius of magnetic field lines at the midpoint of the loop. In the linear regime, R decreases with time (or height), $R_l = (\lambda/2\pi)^2/z$, while R increases with time (height), $R_n = cz$ (Fig. 6). The transition from the linear regime to the nonlinear regime occurs when the two radii become equal, $R_l = R_n$. This occurs at the height $z = z_c = \lambda/(2\pi c^{1/2})$, where the curvature radius is $R = R_c = c^{1/2}\lambda/2\pi$. In our model, $z_c \simeq 3$, because $\lambda = 20$ and c is of order of unity. The actual curvature radius in the simulation results at $z \sim z_c$ is not equal to R_c, but is somewhat larger than R_c and is nearly constant ($\simeq R_0$) near z_c. This stage (called Stage II) corresponds to the nonlinear stage characterized by the exponential expansion of magnetic loops (Fig. 6). When R begins to increase with height, the nature of the magnetic loop expansion gradually changes from the exponential to the power-law type expansion. In Sec. 6.5., we will calculate the second critical height z_t beyond which the solution has the power-law time dependence.

B. Non-Equilibrium in Magnetic Flux in Nonlinear Stage of the Undular Magnetic Buoyancy Instability in Isothermal Layer

We here discuss why the magnetic flux expansion initiated by the undular instability does not decelerate in an isothermal layer in the nonlinear stage. First, we should note that the vertical thickness (D) of our flux sheet is not thin; $D = 4H > H$, where $H = C_s^2/(\gamma g)$ is the pressure scale height. Therefore, the thin tube approximation ($D \ll H$) cannot be used; i.e., $B \neq$ constant inside the flux sheet. Secondly, we note $\beta = 1$ initially, so that the magnetic pressure cannot be assumed to be a perturbation. For these reasons, we have to consider internal structure of the flux sheet as shown in Fig. 7. The expanding flux sheet may be approximated by a current free (potential) magnetic field because plasma pressure (or, equivalently plasma β) is decreased inside the flux sheet owing to the downflow along the field line. If the potential field is approximated by the field illustrated in Fig. 8, the field strength at the midpoint of the loops is $B_x \propto \exp(-z/H_m)$, where $H_m = \lambda/\pi = 6.4H$. Thus the magnetic pressure decreases with height; $p_m \propto \exp(-2z/H_m) = \exp[-z/(3.2H)]$. On the other hand, the gas pressure outside the magnetic flux decreases with height as $p_g \propto \exp(-z/H)$. Consequently, if $\beta = 1$ at the base of the flux sheet, the magnetic pressure at the top of the loop cannot be balanced with the outside gas pressure. This is the reason why there is no saturation (or non-equilibrium) in the nonlinear stage as long as the gas layer is isothermal. There is a critical horizontal wavelength, $\lambda_c = 2\pi H$, beyond which there is no equilibrium state. In other words, the necessary condition for the non-equilibrium is

$$\lambda > \lambda_2 = \pi H \ . \tag{94}$$

In our case, $\lambda = 20H$, and hence this condition is satisfied. [For more exact treatment, see Ref. 15]. It is interesting to note that the above condition is the same as that for the thin tube.[3]

C. Nonlinear Evolution in Stage II: Exponential Expansion

In this subsection, we consider the nonlinear evolution of magnetic loop expansion in stage II around $z \sim z_c$ (Fig. 6), and derive basic formulae found in numerical and analytical studies in Secs. 4 and 5, using an idealized model illustrated in Fig. 9.

We first consider the motion of a fluid element at s along the magnetic loop, where s is the distance from the loop top along the loop. If the gas pressure is neglected, the fluid element falls freely along the loop due to gravity. The equation of motion along the loop is written as

$$dV_s/dt = d^2s/dt^2 = g\sin\theta \simeq g\theta \simeq gs/R \ , \tag{95}$$

for $\theta \ll 1$. If $R \simeq R_0$ is nearly constant in time as discussed in Sec. 6.1, we find

$$s \propto \exp(\Omega t) \ , \tag{96}$$

$$V_s = \Omega s \propto \exp(\Omega t) \ , \tag{97}$$

where

$$\Omega = (g/R_0)^{1/2} \ . \tag{98}$$

We next consider the vertical motion of a local part of the loop (shaded area in Fig. 9) near the midpoint of the loop, and assume $V_z = az$ in Eulerian coordinate and thus $V_z \propto \exp(at)$ in Lagrangian coordinate on the basis of numerical results in Sec. 4. The cross-sectional area of the loop is A, and by assumption $V_z = dA/dt$ and $A \propto \exp(at)$. From conservations of magnetic flux and mass, we have $B_s = 1/A \propto \exp(-at)$ and ρAs=constant, respectively. Then the density inside the shaded area decreases with time as

$$\rho \propto \exp[-(\Omega + a)t] \ . \tag{99}$$

The relation between a and Ω is found from the consideration of the equation of motion in z-direction,

$$\frac{\partial V_z}{\partial t} = -g - \frac{1}{\rho}\frac{\partial p}{\partial z} - \frac{1}{\rho}\left[\frac{\partial}{\partial z}\left(\frac{{B_s}^2}{8\pi}\right) + \frac{{B_s}^2}{4\pi R}\right] \ . \tag{100}$$

The term in the left hand side scales as $\exp(at)$ by the assumption $V_z \propto \exp(at)$. The first term in the right hand side, i.e., the gravitational force term, is constant in time. The second term (the gas pressure force) scales as $\propto \exp(-at)$, and the third term (the magnetic pressure gradient force) $\propto \exp[(\Omega - 2a)t]$. Since initially the first and second terms are comparable to the third term because $\beta = 1$, the first and second terms can be neglected in the later stage if $\Omega > 2a$. The fourth term (the magnetic tension force) is in proportion to $\exp[(\Omega - a)t]$ if $R = R_0 =$ constant. Although the magnetic tension term increases with time more rapidly than the magnetic pressure term, the former is much smaller than the latter in the early stage, and hence may be neglected before it becomes comparable to the magnetic pressure term. In later phase of Stage II, the tension term has the time dependence of $\propto \exp[(\Omega - 2a)t]$, which is the same as that of the magnetic pressure. Altogether, we find that the left-hand side ($\propto \exp(at)$) should balance with the third term in the right hand side ($\propto \exp[(\Omega - 2a)t]$), and thus $a = \Omega - 2a$, or

$$a = \frac{\Omega}{3} = \frac{1}{3}\left(\frac{g}{R_0}\right)^{1/2} . \tag{101}$$

From this relation, we find that the parameter N introduced in Eq. (22) should be equal to 0;

$$N = 1 + \frac{\partial(\rho V_x)/\partial x}{\partial(\rho V_z)/\partial z} = 1 + (3az^{-4})/(-3az^{-4}) = 0 ,$$

because $\rho \propto \exp[-(\Omega + a)t] = \exp(-4at) \propto z^{-4}$, $V_x = \Omega s \simeq \Omega x = 3ax$, $V_z = az$. Since $\Omega = (g/R_0)^{1/2}$ is of order of the linear growth rate (ω_l) of the undular instability, the nonlinear growth rate $\omega_n = a$ is also of order of the linear growth rate; i.e., $\omega_n \simeq \Omega/3 \sim \omega_l/3$. This explains the numerical results found in Fig. 5. Consequently, one can understand that the exponential time dependence of the physical quantities in the Lagrangian coordinate found in numerical and self-similar solutions originates from the exponential time dependence of the downflow speed along the loop due to gravity as shown in Eq. (98).

D. Nonlinear Evolution in Stage III: Power-law Expansion

As the magnetic tension force becomes comparable to the magnetic pressure force, the nature of the expansion changes. That is, the curvature radius increases with height, and the whole magnetic configuration becomes close to that of the potential magnetic field produced by a line current at $(x, z) = (X_s max/2, 0)$;

$$B_x \propto z/(\Delta x^2 + z^2) \ , \tag{102}$$

$$B_z \propto -\Delta x/(\Delta x^2 + z^2) \ , \tag{103}$$

where $\Delta x = x - X_{\rm max}/2$. The distribution of B_x at the midpoint of the loop (Δx=0) in Stage II already has the same distribution $B_x \propto 1/z$ as that given by Eq. (102).

We now show the reason why the expansion law changes from the exponential to the power-law one. Suppose that the curvature radius R is in proportion to s. In this case, we have

$$\frac{d^2 s}{dt^2} \simeq g\frac{s}{R} \simeq g_0 \ , \tag{104}$$

where $g_0 = gs/R =$ constant. Then we find $s = g_0 t^2/2$ and

$$V_s = g_0 t = 2s/t \ . \tag{105}$$

This has the power-law time dependence, and this may be the origin of the power-law expansion of the magnetic flux. On the other hand, the equation of motion vertical to the loop is

$$dV_z/dt = -\frac{1}{\rho}\left[\frac{\partial}{\partial z}\left(\frac{B^2}{8\pi}\right) - \frac{B^2}{4\pi R}\right] \ .$$

If the right-hand side is exactly equal to zero, i.e., if the magnetic field is exactly the potential field, we have also the power-law solution for V_z;

$$V_z = V_0 = z/t \ . \tag{106}$$

These solution satisfies the mass continuity equation

$$\frac{\partial \rho}{\partial t} = -\frac{\partial}{\partial s}(\rho V_s) - \frac{\partial}{\partial z}(\rho V_z) - \frac{\rho V_z}{R} , \tag{107}$$

if

$$\rho = \rho_0 z^{-4} ,$$

where ρ_0 is a constant. Note that we assume $z = r$ and $R = r$ in Eq. (107) where r is the radial distance from the origin $(x, z) = (X_{\max}/2, 0)$ in the cylindrical coordinate (r, θ). The distribution of B_x in the potential field (Eqs. [102] and [103]) also satisfies the induction equation (see Eq. [21]). Consequently, we find that the power-law solutions discussed here correspond to one of the power-law solutions discussed in Sec. 5.2 (the case of $\beta = -4$ and $N = 0$ in Eqs. (91)–(93); see also Table 1).

E. The Second Critical Height z_t and the Maximum Velocity of the Magnetic Loop

We calculate the second critical height z_t between Stages II and III (Fig. 6). This height corresponds to the height where the curvature radius ($R_n = cz$) of magnetic field lines in nonlinearly expanding magnetic flux becomes equal to R_0. Thus we have

$$z_t = R_0/c . \tag{108}$$

To calculate z_t as a function of β_* and H, we use the relation between the nonlinear and linear growth rates,

$$\Omega/3 \sim \omega_l/2 . \tag{109}$$

By using Eq. (98), $\Omega = (g/R_0)^{1/2}$, and the approximate analytical expression for the linear growth rate (for $\beta_* \leq 2$) in Eq. (15), $\omega_l \simeq 0.2(1 + 2\beta_*)^{-1/2} C_s/H$, we find

$$R_0 \simeq 10(1 + 2\beta_*)H . \tag{110}$$

When $\beta_* \simeq 1$, we find $R_0 \simeq 30H$ and thus $z_t \simeq 30H/c \sim 30H$ if $c \sim 1$. This value seems to be consistent with the approximate critical height found in numerical simulations (see Fig. 4).

Since the Stage III has not yet been studied in detail by nonlinear simulations because of some numerical difficulties, it may be premature to discuss the properties of the power-law solution shown in the previous subsection. Therefore we here discuss only that there is a maximum velocity ($V_{\rm max}$) of the magnetic loop expansion, if the analysis in Sec. 6.4 is correct and hence the velocity of the magnetic loop in a Lagrangian frame is nearly constant in Stage III (see Eq. [106]). If the gas layer is isothermal in infinite space, this velocity corresponds to the terminal velocity, and is simply evaluated as

$$V_{\rm max} = a z_t \simeq \frac{1}{2}\omega_l R_0 \simeq (1+2\beta_*)^{1/2} C_s \ , \tag{111}$$

for $\beta_* \leq 2$. Thus the maximum velocity is $\sim 1.7 C_s$ when $\beta_* = 1$, consistent with simulation results.

VII. Summary and Discussion

A. Summary

In this paper, we studied the linear and nonlinear two-dimensional evolution of the undular magnetic buoyancy instability, which is called the ballooning instability in fusion plasma physics and the Parker instability in astrophysics. Main results are summarized in the following:

(1) We first (in Sec. 3) studied the linear characteristics of the undular instability of an isolated horizontal magnetic flux sheet with a vertical thickness $D = 4H$ embedded in an unmagnetized isothermal plasma stratified under constant gravitational acceleration, where H is the pressure scale height in the ambient unmagnetized plasma. We found that the flux sheet is unstable for the long wavelength perturbation with $\mathbf{k} \| \mathbf{B} (\lambda > \lambda_c \simeq 14H)$, and that

the linear growth rate is approximately given by $\omega_l \simeq 0.2(1+2\beta_*)^{-1/2}C_s/H$ for the most unstable wavenumber $k_x \simeq 0.31/H$ and $\beta_* \leq 2$, where β_* is the ratio of gas pressure to magnetic pressure in the initial flux sheet, and C_s is the initial sound speed. The growth rate in a very early stage ($0 \leq t/(H/C_s) \leq 40$; see also Figs. 5 and 6) of the instability in the numerical simulation agrees well with the linear growth rate obtained from a semi-analytical theory.

(2) Numerical simulations (Sec. 4) show that in the early nonlinear stage of the instability ($40 \leq t/(H/C_s) \leq 60$), magnetic loops expand self-similarly with characteristics of the *nonlinear instability* in a Lagrangian frame, because the loop is evacuated by the field aligned motion of matter due to gravity. The rise velocity, V_z, of the magnetic loops and the local Alfven speed, V_A, at the midpoint of the loops increase linearly with height ($V_z \simeq az$, $V_A \simeq a_2 z$), while the density, ρ, and the magnetic field strength,B_x, decrease with height with the power-law distribution ($\rho \propto z^{-4}$, $B_x \propto z^{-1}$). These are nearly steady in an Eulerian frame, but change exponentially with time in a Lagrangian frame. The nonlinear growth rate a is found to be $\sim \omega_l/2$ for $0.5 \leq \beta_* \leq 2$.

A quasi-1D self-similar analytical solution with characteristics of the nonlinear instability in a Lagrangian frame is found (Sec. 5.1), which explains above simulation results very well.

(3) We also find from numerical simulations that in the later stage ($t/(H/C_s) > 60$) of the nonlinear evolution of the instability, the time dependence of the self-similar magnetic loop expansion changes from the exponential to the power-law. This corresponds also to the stage when the magnetic loop enters the hot layer ($z/H > 20$).

More general self-similar analysis in the cylindrical coordinate (Sec. 5.2) shows that there are in fact several self-similar solutions with power-law time dependence (Table 1). One of the solutions (a force-free solution with $N \simeq 0, \beta = -4$) has the characteristics that $V_r \propto r/t$, $\rho \propto r^{-4}$, $B_\theta \propto r^{-1}$, and seems to explain the simulation results in the later nonlinear stage. (Note that $r \simeq z$ for $|\theta| \ll 1$.) The force-free solution with $N = 1$ (i.e., without downflow

along magnetic loops) correspond to the one-dimensional version of two-dimensional self-similar solutions studied by Low.[14]

(4) A simple phenomenological theory is developed to explain simulation and analytical results (Sec. 6). This theory shows that the three different evolutional stages (linear, nonlinear-exponential, nonlinear-power law) are classified by the curvature radius, R, of the magnetic field lines at the top of the magnetic loop (see Fig. 6). The exponential stage is characterized by $R \sim$ constant, while the power-law stage by $R \propto z$. The difference of the time dependence between two nonlinear stages is likely to come from the difference of the nature of the downflow along the magnetic loop; in the exponential case, the downflow speed $V_s \propto \exp(3at)$ for $|\theta| \ll 1$, while in the power-law case $V_s \propto t$. If the power-law solution is exactly equal to the force-free solution, there is a maximum loop speed, $V_{\max} \simeq (1+2\beta_*)^{1/2} C_s$, and the height of transition from the exponential to the power-law (force-free) solution is given by $z_t \simeq 10(1+2\beta_*)H$.

(5) We also found an exact self-similar solution for purely one-dimensional expansion of a magnetized plasma into vacuum without magnetic field when the plasma motion is perpendicular to the magnetic field and there is no gravitational field (Appendix A). The solution has the characteristics that the maximum velocity of plasma is $2V_{A0}$ and time independent, where V_{A0} is the initial Alfven speed of the magnetized plasma. This solution may be useful to understand the results of this paper.

B. Discussion

It is known that the rise velocity V_b of the bubble observed in the laboratory[16] and in the ionosphere[17] tend to be steady in the Lagrangian frame and is in proportion to the radius R_b of the bubble; $V_b = a_3 R_b$, where $a_3 \simeq (1/3 - 1/2) \times (g/R_b)^{1/2}$ is of the order of the linear growth rate of the Rayleigh-Taylor instability. This is similar to our results that $V_z = az \simeq aR$, where R is the curvature radius of the magnetic loop, $a \simeq \omega_l/2$

and ω_l is the linear growth rate. However, the rise velocity of our magnetic loop is not steady in the Lagrangian frame, but increases exponentially with time. This *nonlinear instability* in the Lagrangian frame is also observed in the exact solution found by Ott[18] for the Rayleigh-Taylor instability of a thin, cold gas layer, which is supported against gravity by a hot gas, with a second hot gas above the thin layer.[19] In this case, the growth rate in the nonlinear stage is exactly the same as that in the linear stage. Physically, this is because cold gas in the thin layer freely falls along the curved interface between two hot gases, and mathematically, because the nonlinear basic equations become linear ones in the Lagrangian frame.[20] Although the nonlinear growth rate is not exactly equal to the linear growth rate in our case, the involved physics is common between ours and Ott's problem; the exponential growth in the nonlinear stage is due to the gravitational free fall *along* the magnetic loop. That is, the equation of motion along magnetic loop in our problem is written as $d^2s/dt^2 \simeq (g/R)s$ as shown in Eq. (26), where s is the horizontal distance from the midpoint of the loop. This equation has the exponential solution with the growth rate of $(g/R)^{1/2}$. In addition to this character of *nonlinear instability*, our solution has the *self-similar* property, which is not in Ott's solution.

Finally, we note that the magnetic flux expansion considered in this paper is similar to the free expansion of a magnetized plasma into vacuum in some sense, because the magnetic pressure at the top of the magnetic flux is much larger than the ambient gas pressure. There is, however, one important difference between our case and the pure one-dimensional expansion of a magnetized plasma where there is no gravity and hence the plasma flow vector is exactly perpendicular to field lines (Appendix A); in the latter case, the expansion velocity is constant, while in our case the velocity increases with time (or height) in the exponential phase (Stage II in Fig. 6). This is because the magnetic loop is evacuated by the downflow due to gravity along the loop, which increases the local Alfven speed inside the loop. If there is a high pressure plasma above the expanding magnetic flux, the acceleration

of the magnetic loop soon ceases, and the entire flux is decelerated to find a final equilibrium state.[10]

The authors thank Drs. W. Horton, J. Van Dam, R. Steinolfson, R. Rosner, M. Nambu, and B.C. Low for useful discussions. Computations were performed on FACOM VP200 at the Institute of Plasma Physics, Nagoya University. This work is supported by NSF, NASA and USDOE.

Appendix A

Self-Similar Solutions for 1-D MHD Free Expansion

We present in this Appendix a self-similar solution for the one-dimensional expansion of magnetized cold gas into vacuum.

The problem may be described as follows. Initially, a static gas layer with uniform density ρ_0 is situated in a half space ($z \leq 0$). A uniform horizontal magnetic field B_{x0} penetrates the gas layer. The region $z > 0$ is a vacuum, where there is also no magnetic field. The magnetized gas then expands into the vacuum due to the magnetic pressure gradient, and a rarefaction wave propagates back into the static magnetized gas layer. We assume that gas pressure and gravitational forces are zero, and that the magnetic field is frozen into the gas.

Since this problem contains a characteristic velocity V_{A0}, the initial Alfven speed in the magnetized gas layer, the scaling function Z in Appendix A may be written as

$$Z = V_{A0} t \ , \tag{A1}$$

where

$$V_{A0} = \frac{B_{x0}}{(4\pi\rho_0)^{1/2}} \ . \tag{A2}$$

It is apparent that the gas motion is one-dimensional, $\partial/\partial x = \partial/\partial y = V_x = V_y = 0$. We can then take $N = 1$ and $c = \infty$ in Eqs. (33)–(35), and can omit the curvature term Nv/ζ in

(33). (Note that r in Sec. 5.2 corresponds to z here.) We also assume that Σ in Eq. (31) is independent of time and is equal to ρ_0. Equations (30)–(32) then read

$$V_z = V_{A0} v(\zeta) \ , \tag{A3}$$

$$\rho = \rho_0 \sigma(\zeta) \ , \tag{A4}$$

$$B_x = B_{x0} b(\zeta) \ , \tag{A5}$$

where $\zeta = z/V_{A0}t$.

Basic Eqs. (33)–(35) may be written as

$$v' + (v - \zeta)\frac{\sigma'}{\sigma} = 0 \ , \tag{A6}$$

$$(v - \zeta)v' + \frac{bb'}{\sigma} = 0 \ , \tag{A7}$$

$$(v - \zeta)\frac{b'}{b} + v' = 0 \ . \tag{A8}$$

Boundary conditions are given by

$$v(\zeta = -1) = 0 \ , \tag{A9}$$

$$\sigma(\zeta = -1) = 1 \ , \tag{A10}$$

$$b(\zeta = -1) = 1 \ , \tag{A11}$$

because $\zeta = -1$ corresponds to the front of the rarefaction wave propagating into the initial static magnetized gas layer.

From Eqs. (A6) and (A8), we find

$$b = \sigma \ , \tag{A12}$$

by using boundary conditions (A10) and (A11). From Eqs. (A6), (A7) and (A12), we obtain

$$\sigma = (\zeta - v)^2 \ . \tag{A13}$$

Inserting equation (A13) into Eq. (A6), it follows that

$$v' = \frac{2}{3} . \tag{A14}$$

Thus, using boundary condition (A9), we have the solution

$$v = \frac{2}{3}(\zeta + 1) . \tag{A15}$$

The equation (A13) then leads to

$$\sigma = b = \frac{1}{9}(\zeta - 2)^2 . \tag{A16}$$

The solution can now be summarized as

$$V_z = \frac{2}{3} V_{A0} \left(\frac{z}{V_{A0} t} + 1 \right) , \tag{A17}$$

$$\rho = \frac{1}{9} \rho_0 \left(\frac{z}{V_{A0} t} - 2 \right)^2 , \tag{A18}$$

$$B_x = \frac{1}{9} B_{x0} \left(\frac{z}{V_{A0} t} = -2 \right)^2 . \tag{A19}$$

The region where this solution is applicable is $-1 \leq z/V_{A0}t \leq 2$. Note that the maximum velocity is constant, $2V_{A0}$, at $z = 2V_{A0}t$.

References

1. M.D. Kruskal and M. Schwartzschild, Proc. Roy. Soc. London **23A**, 348 (1954).

2. H.K. Moffat, *Magnetic Field Generation in Electrically Conducting Fluids*, (Cambridge: Univ. Press, 1978); E.R. Priest, *Solar Magnetohydrodynamics* (Dordrecht: Reidel, 1982), p. 293; D. W. Hughes and M.R.E. Proctor, *Ann. Rev. Fluid Mech.* **20**, 187.

3. E.N. Parker, *Cosmical Magnetic Field* (Oxford: Clarendon Press, 1979), p. 314.

4. W.A. Newcomb, Phys. Fluids **4**, 391 (1961).

5. E.N. Parker, Astrophys. J. **145**, 811 (1966).

6. B. Coppi and M.N. Rosenbluth, in *Plasma Phys. and Cont. Nucl. Fus. Res.* Vol. 1, (IAEA, Vienna, 1966), p. 617.

7. As for the nonlinear simulations of ballooning instability, see e.g., T. Ogino, H. Sanuki, T. Kamimura, and S. Takeda, J. Phys. Soc. Jpn. **50**, 1698 (1981); F. Brunel, J.-N. Leboeuf, T. Tajima., and J.M. Dawson, J. Comp. Phys. **43**, 268 (1981).

8. T. Horiuchi, R. Matsumoto, T. Hanawa, and K. Shibata, Publ. Astr. Soc. Jpn. **40**, 147 (1988).

9. R. Matsumoto, T. Horiuchi, K. Shibata, and T. Hanawa, Publ. Astr. Soc. Jpn. **40**, 171 (1988).

10. K. Shibata, T. Tajima, R. Matsumoto, T. Horiuchi, T. Hanawa, R. Rosner, and Y. Uchida, Astrophys. J. **338**, 471 (1989).

11. Ya. B. Zeldovich and Yu. P. Raizer, *Physics of Shock Waves and High Temperature Hydrodynamic Phenomena* (New York: Academic, 1967), Vol. 2; L.I. Sedov, *Similarity and Dimensional Methods in Mechanics*, (New York: Academic, 1959).

12. Self-similar analyses for Z-pinch have been performed by F.S. Felber, Phys. Fluids, **25**, 643 (1982); P. Rosenau, R.A. Nebel, and H.R. Lewis, Phys. Fluids **B1**, 1233 (1989).

13. H. Kull, Phys. Fluids **B1**, 170 (1989).

14. B.C. Low, Astrophys. J. **254**, 796 (1982); **261**, 351 (1982); **281**, 381, 392 (1984).

15. B.C. Low, Astrophys. J. **251**, 352 (1981).

16. R.M. Davies and G.I. Taylor, Proc. Roy. Soc. London **A200**, 375 (1950); D.H. Sharp, Physica **12D**, 3 (1984).

17. e.g. P.K. Chaturvedi and P.K. Kaw, Geophys. Res. Lett. **2**, 381 (1975); M.C. Kelly *et al.*, Geophys. Res. Lett. **3**, 448 (1976); P.K. Chaturvedi and S L. Ossakow, Geophys. Res. Lett. **4** 558 (1977); S.L. Ossakow and P.K. Chatuvedi, J. Geophys. Res. **83**, 2085 (1978); E. Ott, J. Geophys. Res. **83**, 2066 (1978).

18. E. Ott, Phys. Rev. Lett. **29**, 1429 (1972).

19. See some related studies, e.g., D. Colombant, W. Manheimer, and E. Ott, Phys. Rev. Lett. **53**, 446; E. Infeld and G. Rowlands, Phys. Rev. Lett. **60**, 2273.

20. J.M. Dawson, Phys. Rev. **113**, 383 (1959); R.C. Davidson, *Methods in Nonlinear Plasma Theory*, (New York: Academic, 1972), p. 35.

Figure Captions

1. Linear growth rate ($i\omega$) of the undular mode of the magnetic buoyancy instability in the gas layer with an isolated magnetic flux sheet as a function of the horizontal wavenumber k_x. Three cases, $\beta_* = 0.5$, 1.0, and 2.0, are shown for $k_y = 0$.

2. The z-distribution of the linear eigenfunction in the case of $k_x = 0.314$ and $k_y = 0$. The magnitudes are normalized so that $(i\tilde{v}_x/C_s)_{\max} = 1$.

3. Simulation results; (a) the magnetic field lines $\mathbf{B} = (B_x, B_z)$, (b) the velocity vector $\mathbf{V} = (V_x, V_z)$, (c) density contours ($\log \rho$).

4. The distributions in z of (a) the vertical velocity V_z, (b) the local Alfvén speed V_A, (c) the horizontal magnetic field ($\log B_x$), (d) the density ($\log \rho$) at $x = X_{\max}/2 = 40$. The numbers attached to the curves correspond to the following time (in unit of H/C_s); (1) $t = 42.1$, (2) 49.6, (3) 57.6, (4) 64.6.

5. The time evolution of Lagrangian displacement ($\Delta z_m = z_m(t) - z_m(0)$; solid curve) of a test particle. The dashed line shows the linear growth with $\omega_l = 0.121 C_s/H$, and the dash-dotted line shows the nonlinear growth with $\omega_n = 0.06 C_s/H$.

6. The schematic picture of the curvature radius R of a magnetic field line as a function of the height z, and the classification of the evolutionary stages: I (linear), II (nonlinear; exponential time dependence), and III (nonlinear; power-law time dependence). The solid curve shows the actual (but not exact) curvature radius of a rising magnetic loop, the dashed curve with $R = (\lambda/2\pi)^2/z$ corresponds to the curvature radius of a loop in the linear regime, and another dashed line ($R = cz$) shows that of the nonlinear stage.

7. Schematic illustration of the expanding magnetic flux as a result of the undular mode of the magnetic buoyancy instability with wavelength λ. Note that the thickness of the sheet D is much larger than the pressure scale height H outside the flux sheet.

8. An example of the potential magnetic field when the horizontal wavelength is fixed to λ even in the nonlinear stage.

9. An idealized model for the rising magnetic loop with downflow along it due to gravity.

Summary of Self-Similar Solutions

$Z\ddot{Z}/\dot{Z}^2 \neq 1$	$\delta \neq 1$	$N \neq 0$	no solution
		$N = 0$	$V_r \propto \tau^{\delta/(1-\delta)}\zeta^{\delta} \propto r^{\delta}$ $B_\theta \propto \tau^{-\delta/(1-\delta)}\zeta^{-\delta} \propto r^{-\delta}$ $\rho \propto \tau^{-4\delta/(1-\delta)}\zeta^{-4\delta} \propto r^{-4\delta}$ $\alpha = 1/(1-\delta)$
cline2-4 $[Z \propto \tau^{\alpha}]$	$\delta = 1$	$N \neq 1$	$V_r \propto \tau^{\alpha-1}\zeta^{\alpha} \propto r/t$ $B_\theta \propto \tau^{-\alpha}\zeta^{-1-h} \propto t^{-h\alpha}r^{-1-h}$ $\rho \propto \tau^{2-4\alpha}\zeta^{-4-2h} \propto t^{2(1+h\alpha)}r^{-4-2h}$ where $h = (N-1/\alpha)/(1-N)$
		$N = 1$	same as the force-free solution
$Z\ddot{Z}/\dot{Z}^2 = 1$	$\delta \neq 1$	any N	no solution
$[Z \propto \exp(a\tau)]$	$\delta = 1$	$N \neq 1$	$V_r \propto \zeta \exp(a\tau) \propto r$ $B_\theta \propto \zeta^{-1-p}\exp(-a\tau) \propto r^{-1-p}\exp(pat)$ $\rho \propto \zeta^{-4-2p}\exp(-a\tau) \propto r^{-4-2p}\exp(2pat)$ where $p = N/(1-N)$
		$N = 1$	no solution
force-free $[Z \propto \tau]$	$\delta = 1$	$N = 1$	$V_r \propto \zeta \propto r/t$ $B_\theta \propto \tau^{-1}\zeta^{-1} \propto r^{-1}$ $\rho \propto \tau^{-2}\zeta^{-\mu} \propto t^{\mu-2}r^{-\mu}$ $\alpha = 1, c = 1, \mu =$ arbitrary
		$N \neq 1$	$V_r \propto \zeta \propto r/t$ $B_\theta \propto \tau^{-1}\zeta^{-1} \propto r^{-1}$ $\rho \propto \tau^{\beta}\zeta^{\beta+w} \propto t^{-w}r^{\beta+w}$ $w = (\beta+2)N/(1-N)$ $\alpha = 1, c = 1, \mu =$ arbitrary

Table I Note: $\zeta = r/Z(\tau)$ is Lagrangian coordinate, r is Eulerian coordinate (height measured from the base of the initial magnetic flux tube), $r \simeq z$ for $|\theta| \ll 1$, and δ is the exponent of velocity function ($V_r \propto r^{\delta}$).

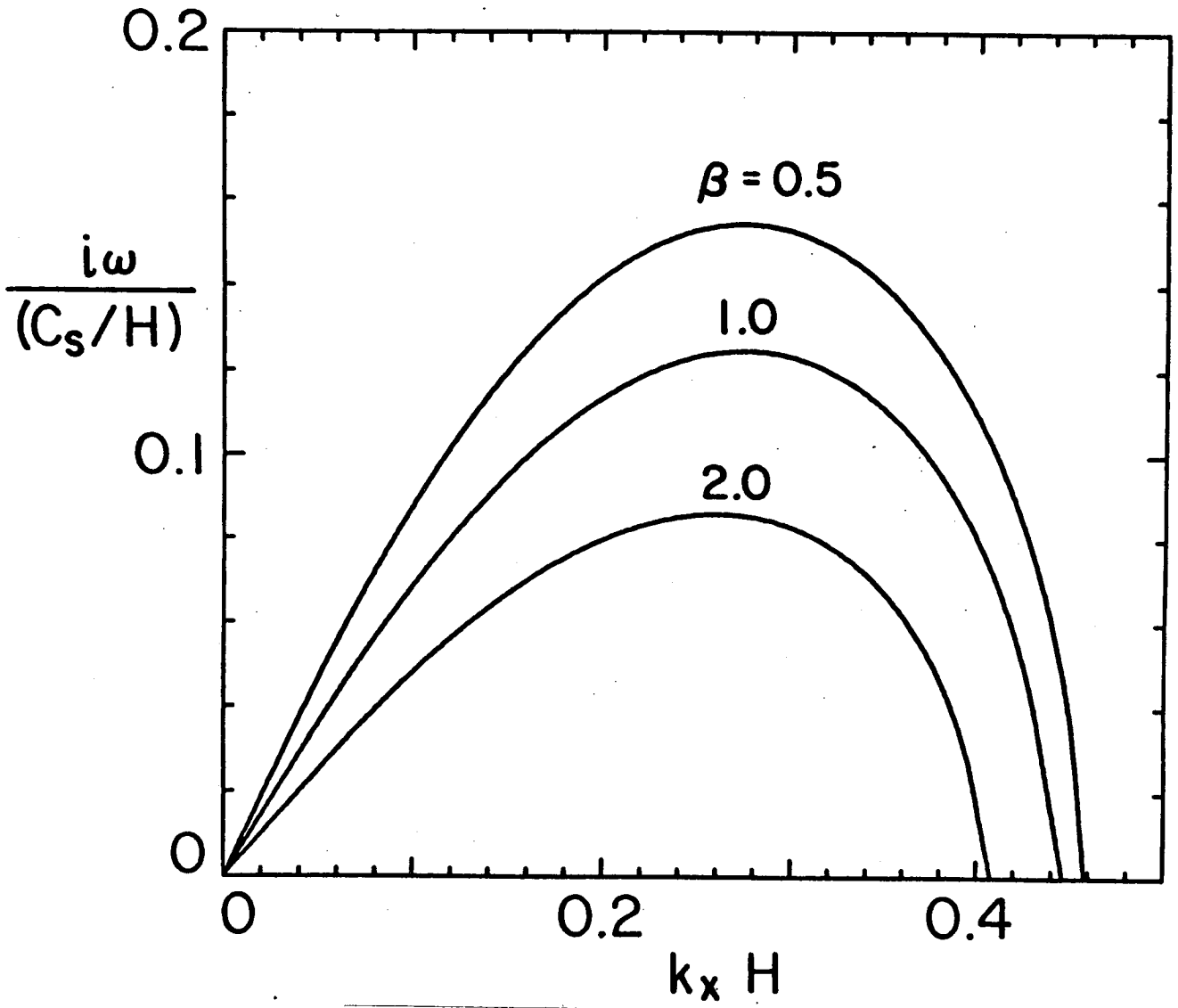

Fig. 1

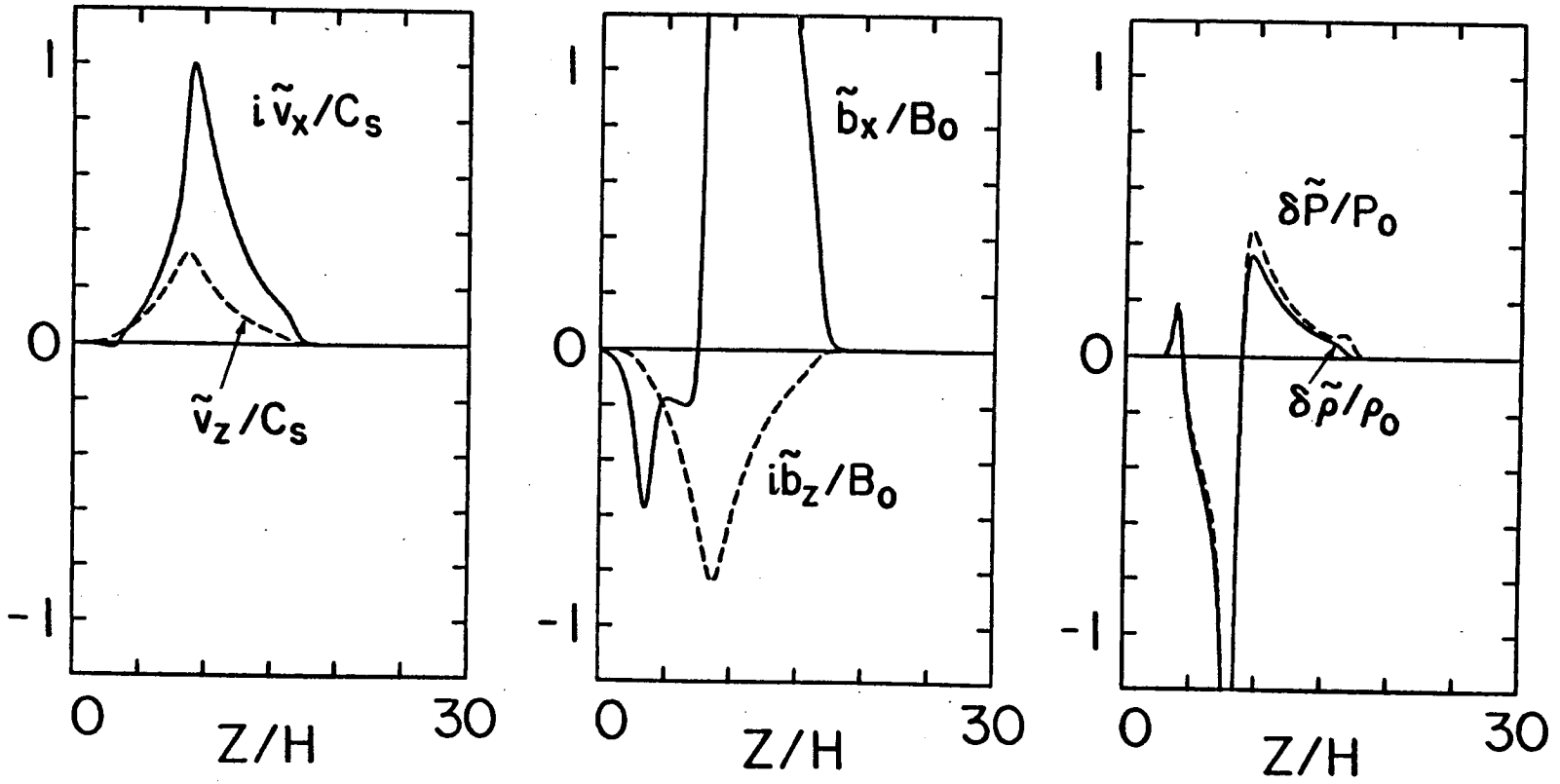
1
0
-1
$i\tilde{v}_x/C_s$
$\tilde{v}_z/C_s$
0
Z/H
30
1
0
-1
$\tilde{b}_x/B_o$
$i\tilde{b}_z/B_o$
0
Z/H
30
1
0
-1
$\delta\tilde{P}/P_o$
$\delta\tilde{\rho}/\rho_o$
0
Z/H
30

Fig. 2

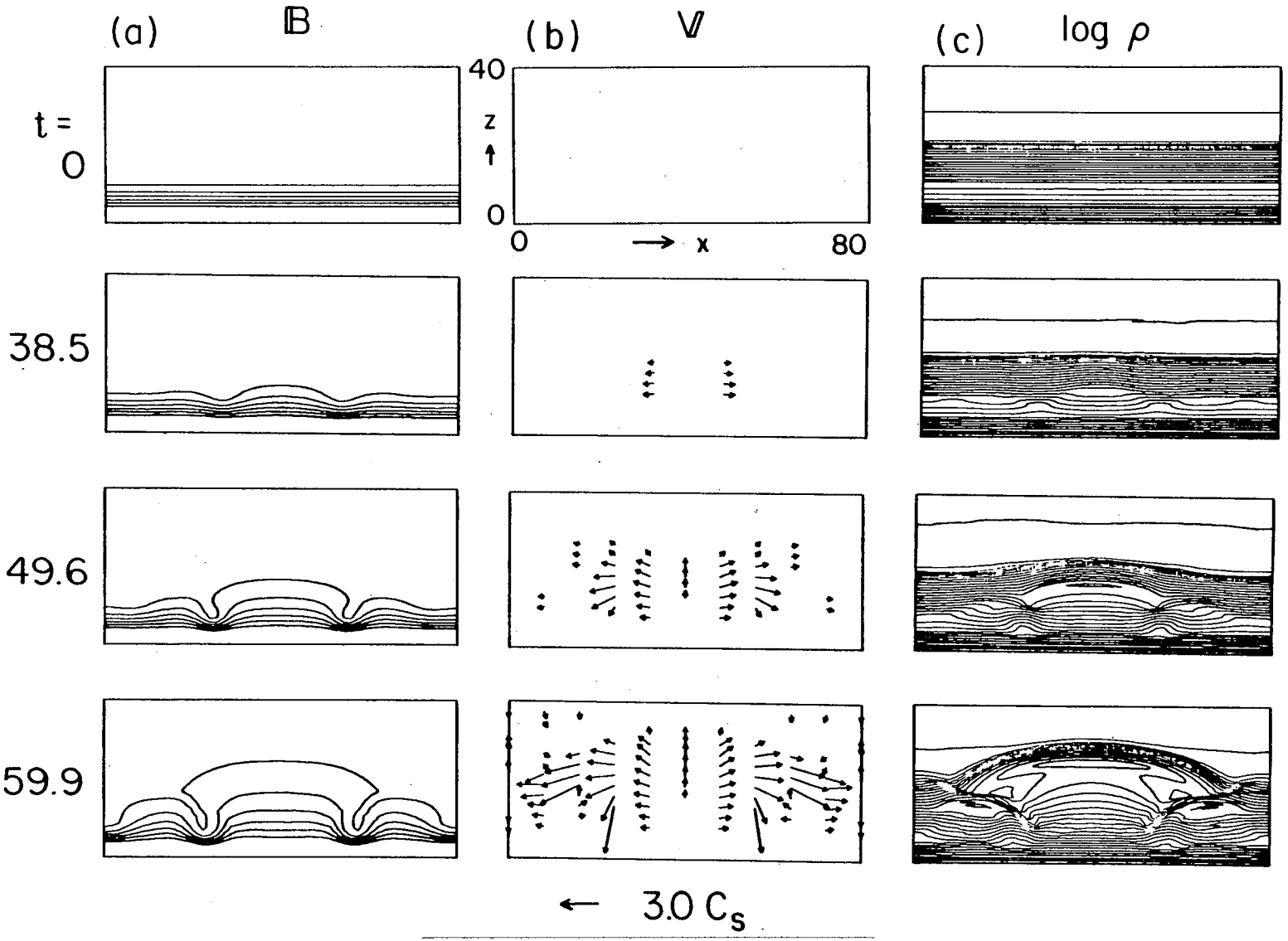

Fig. 3

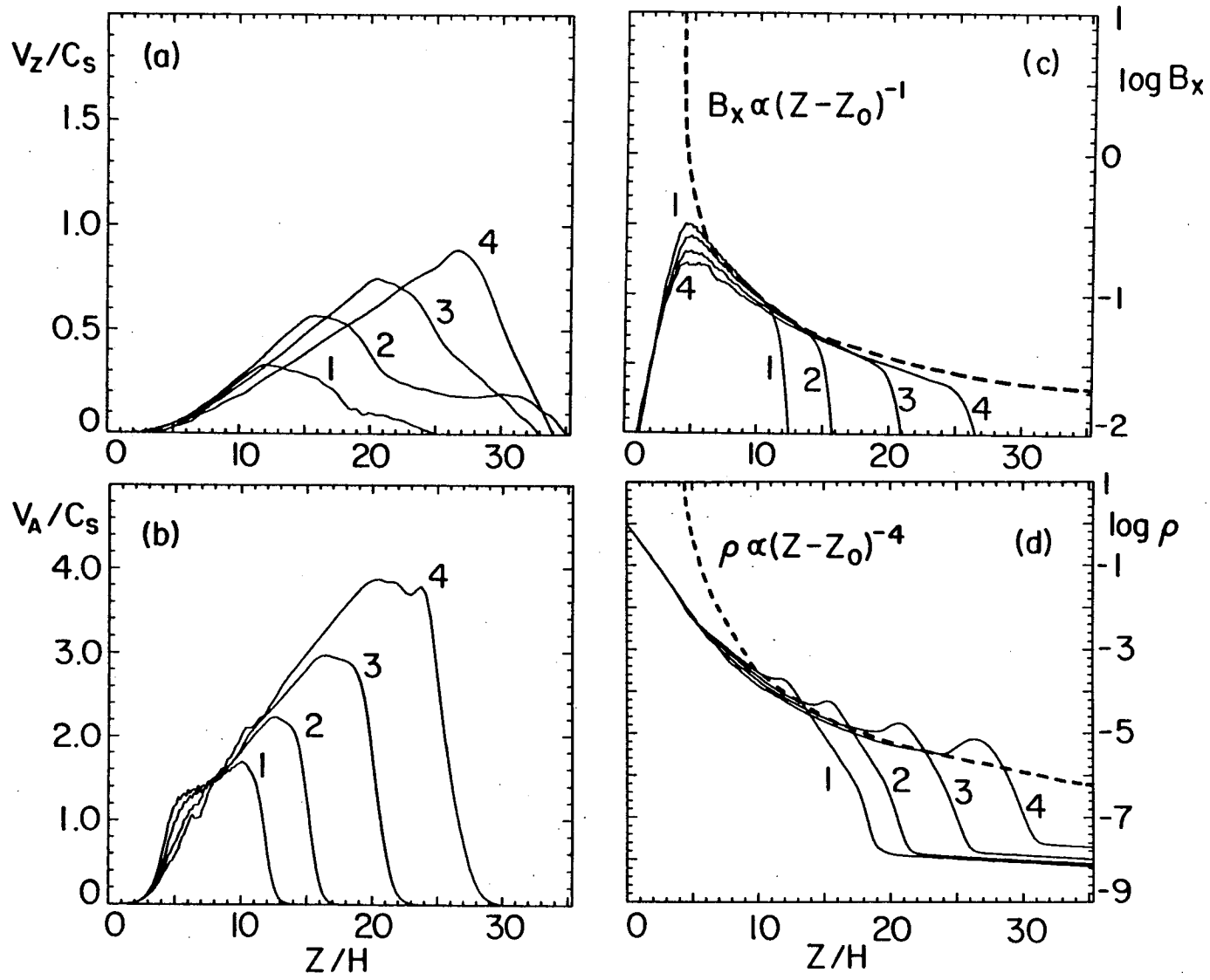
V_z/C_s
(a)
1.5
1.0
0.5
0
0
10
20
30
1
2
3
4
$B_x \propto (Z-Z_0)^{-1}$
(c)
log B_x
1
0
-1
-2
V_A/C_s
(b)
4.0
3.0
2.0
1.0
Z/H
$\rho \propto (Z-Z_0)^{-4}$
(d)
log ρ
-1
-3
-5
-7
-9

Fig. 4

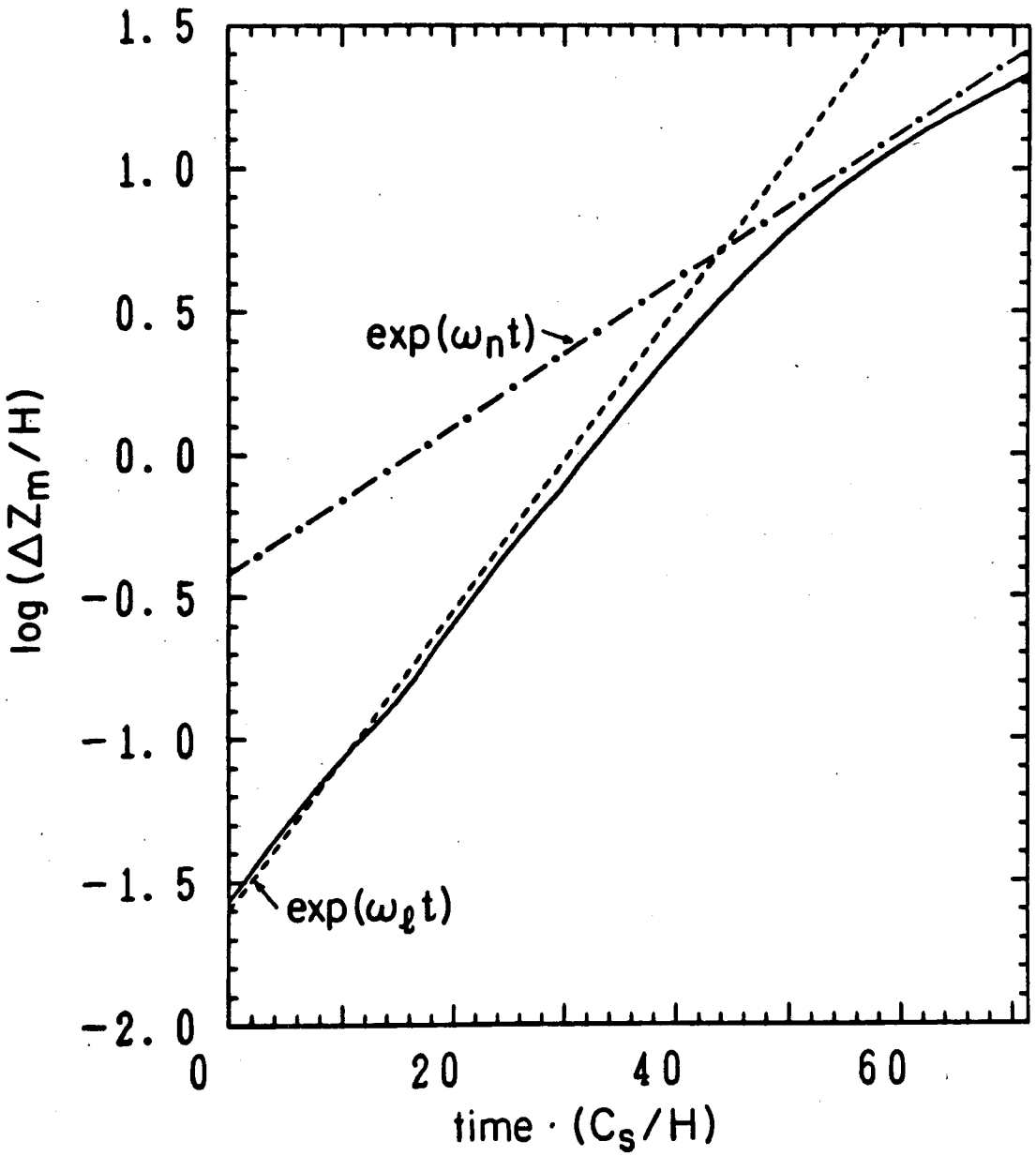

Fig. 5

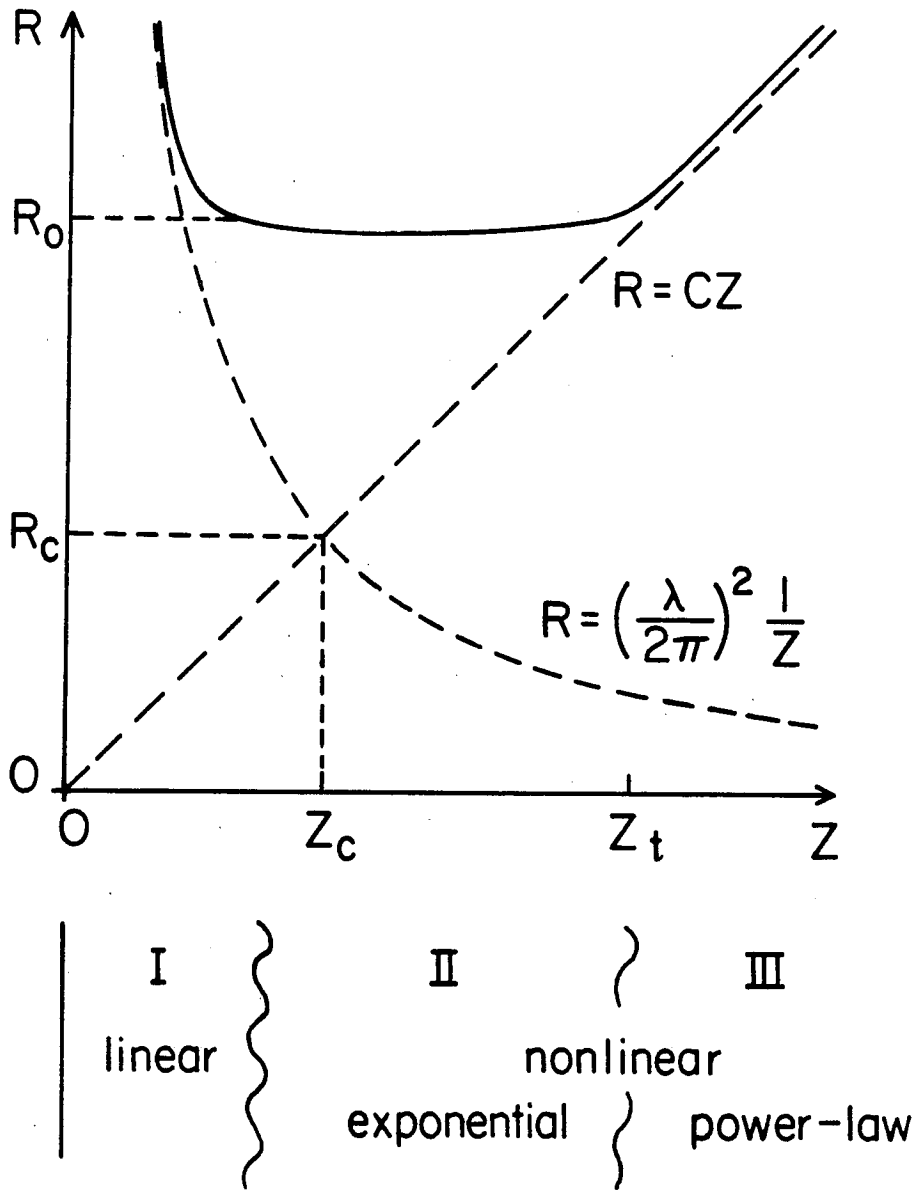
R
R_o
R_c
O
O
Z_c
Z_t
Z
R = CZ
$R = \left(\frac{\lambda}{2\pi}\right)^2 \frac{1}{Z}$
I
linear
II
nonlinear
exponential
III
power-law

Fig. 6

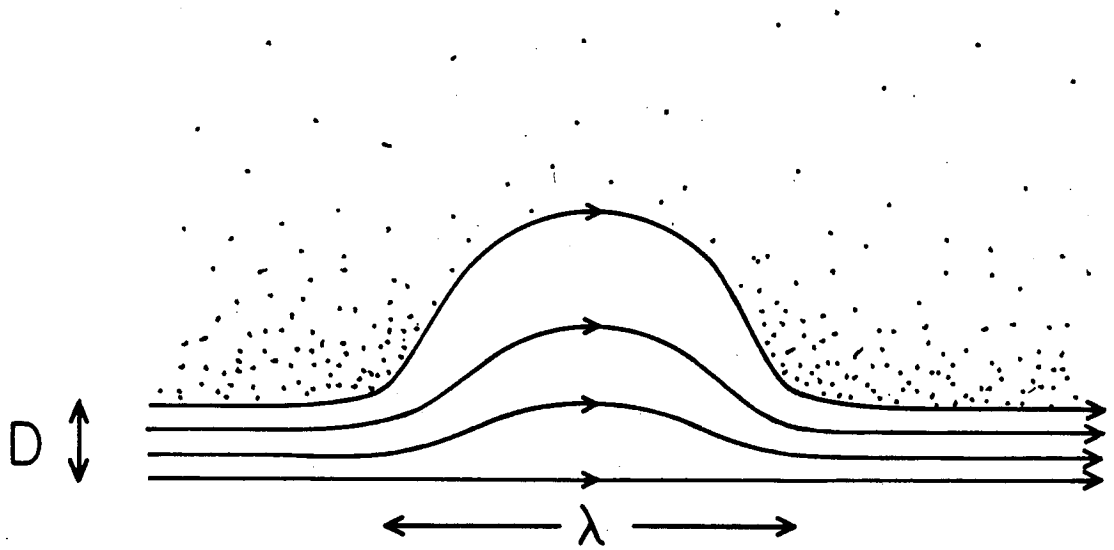

Fig. 7

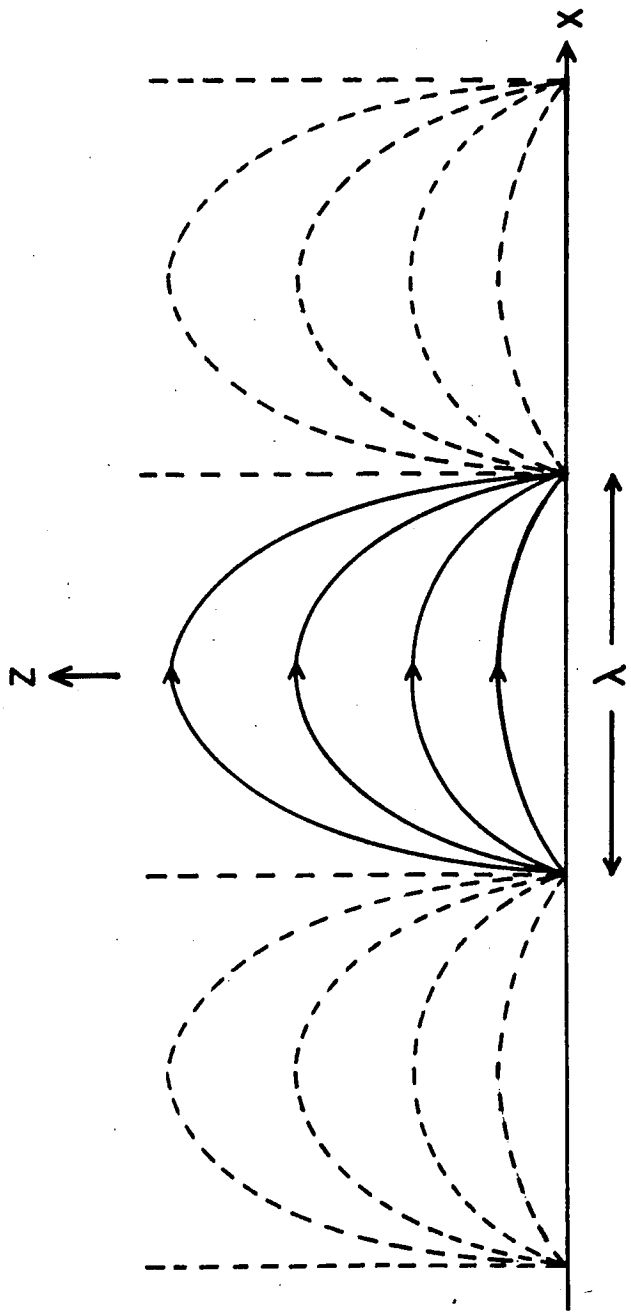

Fig. 8

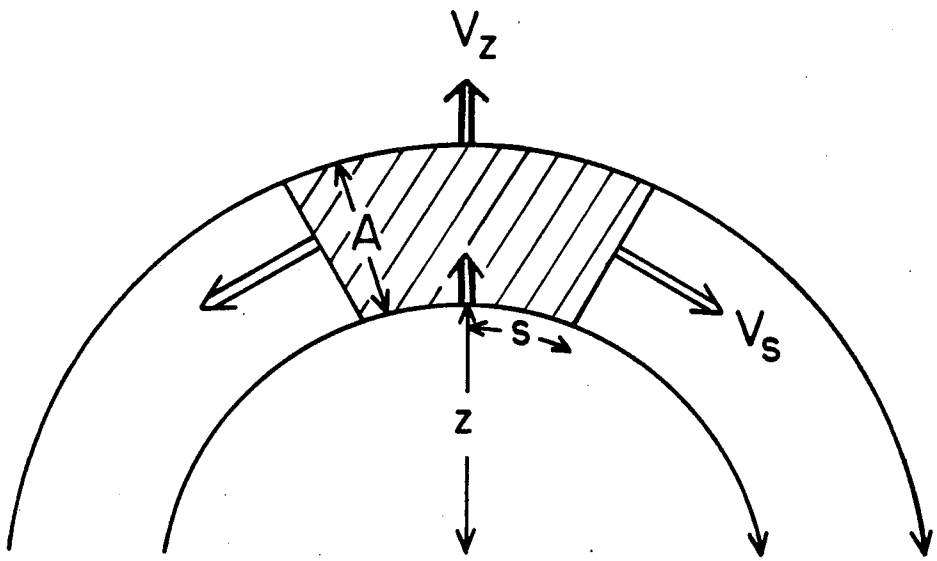

Fig. 9